Mitigating Stress Corrosion Cracking of 304L and 316L Laser Welds by Micro-shot Peening

Chia-Ying Kang , Tai-Cheng Chen , Ren-Kae Shiue , Leu-Wen Tsay *

Posted Date: 27 October 2023

doi: 10.20944/preprints202310.1749.v1

Keywords: cold-rolling, laser weld, micro-shot peening, stress corrosion cracking, pitting corrosion

Article

Mitigating Stress Corrosion Cracking of 304L and 316L Laser Welds by Micro-shot Peening

Chia-Ying Kang [1], Tai-Cheng Chen [2,3], Ren-Kae Shiue [3] and Leu-Wen Tsay [1,*]

[1] Department of Optoelectronics and Materials Technology, National Taiwan Ocean University, Keelung 20224, Taiwan; Tiffany1129.k@gmail.com (C.-Y.K.), b0186@mail.ntou.edu.tw (L.-W.T.)
[2] Department of Material Research, National Atomic Research Institute, Taoyuan 32546, Taiwan; tcchen@nari.org.tw (T.-C.C.)
[3] Department of Materials Science and Engineering, National Taiwan University, Taipei 10617, Taiwan; rkshiue@ntu.edu.tw (R.-K. S.)
* Correspondence: b0186@mail.ntou.edu.tw (L.-W.T.); Tel.: +886-2-24622192 ext.6405

Abstract: Two austenitic stainless steel (ASS) plates, 304L and 316L, were cold-rolled (304R and 316R) with a 10 % reduction in thickness then subjected to laser welding. Cold-rolling caused a slight surface hardening and introduced residual tensile stress into the ASS plates. The susceptibility to stress corrosion cracking (SCC) of the welds (304RW and 316RW) was determined using the U-bend test pieces in a salt spray. To highlight the stress concentration at the weld's fusion boundary (FB), the top weld reinforcement was not ground off before bending. Moreover, micro-shot peening (MSP) was performed to mitigate the SCC of the welds by imposing high residual compressive stress and forming a fine-grained structure. Cold-rolling increased the susceptibility of the 304R specimen to pitting corrosion (PTC) and intergranular (IG) microcracking. Moreover, PTC and SCC were found more often at the FBs of the 304RW. The corrosion pits of the peened 304RW (304RWSP) were finer but greater in amount than the un-peened one. The results also indicated that the 316L ASS welds with MSP was resistant to the incidence of PTC and SCC in a salt spray. The better reliability and longer service life of dry storage canister could be achieved by using 316L ASS for construction and application of MSP on it.

Keywords: cold-rolling; laser weld; micro-shot peening; stress corrosion cracking; pitting corrosion

1. Introduction

Austenitic stainless steels (ASSs) are put in use to construct canister to store low- and medium-level nuclear waste [1-4]. For the building of nuclear waste canister, machining and/or cold-rolling the ASS causes a phase transformation of austenite (γ) to martensite [5-8], while welding thermal cycles introduce residual tensile stress [9-10] into the final product. The introduction of thermal and mechanical treatments will bring out changes in physical and chemical properties of the ASSs. The dry storage canisters are proposed to be placed in the nuclear power station near the coastline in Taiwan. With a saline atmosphere and high humidity, the dry storage canister will confront the problem of chloride-induced corrosion/stress corrosion cracking (SCC). In recent study, synthetic sea-salt, Mg-chlorides and particular salt are deposited on the 316L stainless steel (SS) canister to investigate the SCC susceptibility in distinct zones of the weld [1].

Cold-rolling and subsequent welding are known to bring out a great change in microstructure and corrosion resistance of the ASS welds. The slow strain rate tensile tests in 3.5 % NaCl solution show that the tensile elongation and strength of cold-rolled 304 SS decrease by 81 and 42 %, respectively, compared with the annealed samples [11]. During cyclic loading or cold deformation, the protective film of 316 SS is broken by the induced martensite, resulting in decreasing the corrosion resistance in chlorine-treated water [12]. The induced α'-martensite is found to be the preferential crack path for the 304 SS reactor serviced in the $MgCl_2$ solution [13]. Moreover, the crack growth along the slip lines of the cold-worked 304L SS is much earlier than that of the annealed sample in 1M HCl solution [14]. Aging at elevated temperature or imposing welding cycle will enhance Cr-carbide precipitation at the grain boundaries of the ASS, called sensitization. It is reported that cold-

 doi:10.20944/preprints202310.1749.v1

rolling will results in severe sensitization at the temperature down to 500 ºC [15]. After sensitization at 500 ºC, the prior cold-worked 304 SS suffered from the intergranular SCC in polythionic acid [16]. Furthermore, cold-rolled, sensitized 304L SS shows the high SCC susceptibility in a salt spray at 80 ºC [17]. Therefore, cold-rolling before welding is expected to cause the ASS weld to be sensitive to SCC. By contrast, surface modification processes, likewise shot-peening, are applied to decrease the SCC susceptibility of the ASS welds [18]. Severe shot peening of the 304 SS causes significantly refined grains and introduces residual compressive stress [19]. Ultrasonic surface modification improves the corrosion resistance of 304 SS weld in boiling $MgCl_2$ solution [20]. The weld toe curvature of 304 SS weld can be modified while cracking at the weld toe is eliminated by ultrasonic peening [21]. In case of the annealed 304L plate subjected to laser welding, high local strain at the weld's fusion boundary (FB) shows high susceptibility to SCC [22]. It is reported that better fatigue strength of the butt welds can be obtained by means of shot peening and clean blasting [23].

AISI 304 SS jointed by gas tungsten arc welding (GTAW) process shows high microstructural and mechanical heterogeneity in distinct zones of the weld [24]. To increase the reliability or prolong the service life, the occurrence of PTC/SCC of the dry storage canister in a saline atmosphere has to be suppressed or under control. To access the practical condition, the cold-rolled 304L and 316L plates were welded by CO_2 laser in this study. SCC of the ASS welds were evaluated by using the U-bend test pieces in a salt spray. Micro-shot peening (MSP) was applied on the top weld surface to mitigate the SCC. The damage formed on the surface of the U-bend test pieces was examined by scanning electron microscope (SEM). Both phase transformation and refined microstructure near the peened surface were analyzed using the electron backscatter diffraction (EBSD). The effect of MSP on the microstructure and residual stress distribution of the peened samples were related with the SCC susceptibility of the investigated samples.

2. Materials and Experimental Procedures

Annealed 304L and 316L SS plates with an initial thickness of 3.0 mm were cold-rolled to 2.7 mm in thickness, which was about 10 % reduction in thickness. The cold-rolled 304L and 316L plates were named 304R and 316R, respectively. The 304R and 316R samples were welded by CO_2 laser in keyhole mode in one pass, which was designated to be the 304RW and 316RW, respectively. In case of the sample with MSP, the "SP" would be added to the designated sample. To highlight the stress concentration at the FB, the top weld reinforcement was not ground off before U-bending in this work. Some U-bend test pieces were shot-peened with iron-based amorphous powders [25] under 200 % surface coverage [22]. A Vickers micro-hardness tester was applied to measure the hardness of distinct zones in the weld with a load of 25 gf for 15 sec. X-ray diffraction (XRD) was carried out to examine the phase constitutions of the sample.

A U-bend sample with the dimensions of 10 mm × 120 mm × 2.7 mm was used for SCC evaluation in a salt spray containing 10 % NaCl at 80 ºC. The augmented strain on the top surface of the U-bend test piece is about 13.5 %, which was imposed using a die block of 20 mm in diameter. To examine the corroded appearance of the tested pieces, the samples were periodically removed from the environmental chamber and observed by a microscope. The SCC tests in a salt spray were terminated after 672 h.

Residual stress distributions in cold-rolled plates with or without MSP were measured using a residual stress analyzer. The residual stress in the thickness direction was acquired by eliminating the surface layer of the specimens with the aid of an electrochemical polisher. The corroded appearance of the U-bend specimens after salt spray were observed by an SEM. The strain-induced α'-martensite and refined microstructure formed on the shot-peened layer were explored using the EBSD. Moreover, the strain distribution of the investigated specimen was determined using the HKL Channel 5 software to analyze the original data acquired by the EBSD.

3. Results

3.1. Macro-views of the tested samples

 doi:10.20944/preprints202310.1749.v1

Figure 1 shows the macro-views of the U-bend samples for the salt spray tests, which are the cold-rolled SS plates welded by CO_2 laser. As shown in Figure 1a, the augmented strain was about 13.5 % on the external surface of the smooth sample. In this work, the U-bend weld comprised a weld reinforcement in the middle of the test piece (Figure 1a). The top view of the U-bend weld is shown in Figure 1b, showing the discontinuous profile at the weld's FB (indicated by the arrow). The lateral view of the U-bend weld is shown in Figure 1c. Overall, the weld reinforcement of an autogenous laser weld was still low compared to the conventional arc weld. The construction of the dry storage canister for the spent fuels in Taiwan is by joining the cold-rolled 304/304L plate by arc-welding process into a cylinder of about 1.8 m diameter. The new specification for the construction of the dry storage canister requires to grind off all the weld reinforcement and avoid the undercut of the weld, which has the benefits of reducing the stress concentration and accumulation of contaminants therein.

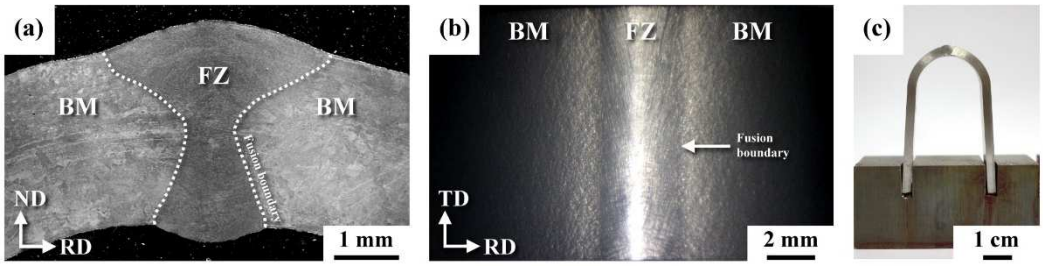

Figure 1. The macroscopic photos of (**a**) the U-bend weld in cross sectional view, (**b**) the top appearance of the U-bend weld, (**c**) the lateral view of the U-bend sample for the salt spray (BM: base metal; FZ: fusion zone).

3.2. XRD spectrums of the cold-rolled samples with and without MSP

The annealed 304L and 316L plates were non-ferromagnetic, i.e., ferrite number (FN) determined by ferrite scope was nearly zero. Cold-rolling of unstable ASSs was expected to cause strain-hardening and strain-induced martensitic transformation. With a 10 % reduction in thickness after cold-rolling, a minor increase in FN from zero to 0.7 was found for the 304R and about 0.1, for the 316R samples. The XRD spectrums of the cold-rolled plates in the as-rolled and shot-peened conditions are shown in Figure 2. The XRD results indicated that no distinguishable ferrite phase was observed in the 304R and 316R samples. After peening, a slightly broaden γ peak was seen in the 304RSP sample, which could be related with the formation of a certain amount of α'-martensite mixed with the γ matrix. By contrast, γ was still the predominant phase in the 316RSP sample. The ferrite scope and XRD spectrum confirmed the 316L SS with high resistance to strain-induced transformation relative to the 304L SS. It is reported that plastic deformation induced by MSP assisted austenite to martensite transformation and strain-hardening within a narrow depth [25]. The microstructure of the cold-rolled ASSs showed traces of slip lines within the granular austenite matrix, especially around the external surface, which were not seen in the annealed plates and would be confirmed in the following EBSD analysis. As reported previously [22], the fusion zone (FZ) of the 304L and 316L welds had a FN of about 1.78 and 0.54, respectively. The high FN of the 304L FZ was associated with the skeletal microstructure with vermicular ferrite (δ) within the solidified matrix, while cellular dendrites with less ferrite are formed in the 316L FZ of low FN [22].

Preprints (www.preprints.org) | NOT PEER-REVIEWED | Posted: 27 October 2023 doi:10.20944/preprints202310.1749.v1

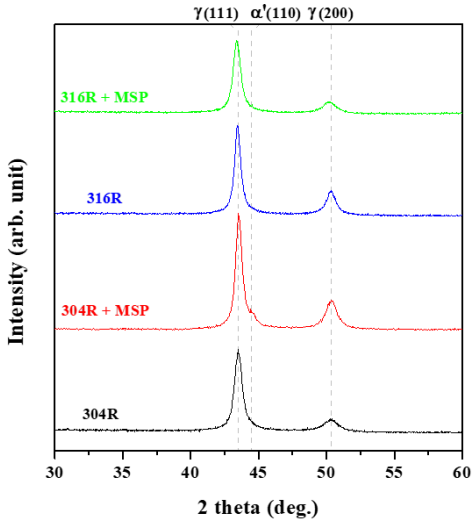

Figure 2. The XRD spectrums of the cold-rolled ASSs in the as-rolled and shot-peened conditions.

3.3. The micro-hardness profiles of the shot-peened welds

The microhardness profiles in distinct zones of two welds are displayed in Figure 3. Each hardness measurement was performed at 5 and 20 μm away from the outer surface of the cold-rolled plates. Cold-rolling resulted in a slight strain-hardening around the surface. Because of the imposed strain-hardening of the cold-rolled plate, the hardness of the FZ was the lowest among the distinct zones in the weld (Figure 3). At the depth 20 μm away from the outer surface of the plate, both FZ and the base metal (BM) had almost identical hardness, regardless of the welds.

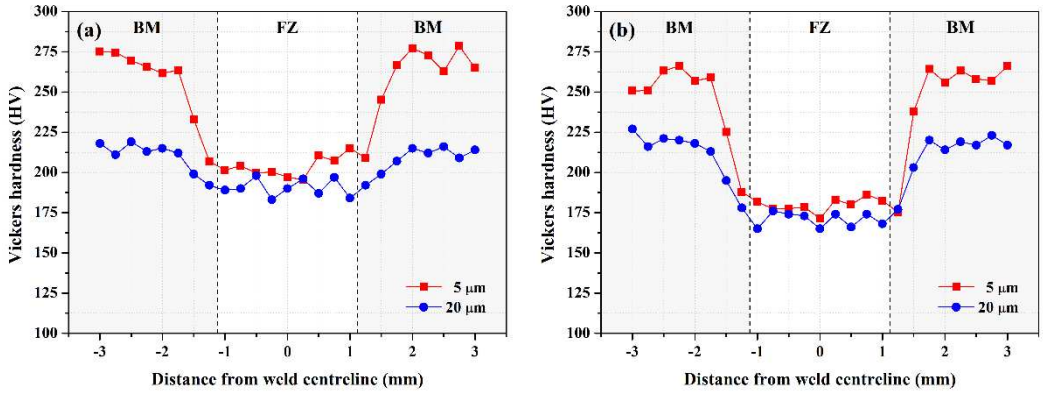

Figure 3. The hardness distributions in distinct zones of the (**a**) 304RW and (**b**) 316RW samples at the depths of 5 and 20 μm from the top surface of the cold-rolled plates.

Figure 4 demonstrates the variations in micro-hardness along the thickness direction in three different zones of the shot-peened welds from the outmost surface to the interior after MSP. According to the hardness profiles, the peen-affected depth was about 70 μm, regardless of the welds after MSP. At a depth of about 70 μm, the FZ, FB and BM all had the similar hardness despite the welds. Around the peened layer, the three different zones in the 304RWSP sample were harder than those in the 316RWSP one in each group after MSP. A marked drop in hardness from about HV 400 to HV 200 was obtained within 70 μm depth for the shot-peened weld. Such high outmost hardness in the FZ, FB and BM might accompany with a great decrease in the PTC and SCC resistance.

Preprints (www.preprints.org) | NOT PEER-REVIEWED | Posted: 27 October 2023 doi:10.20944/preprints202310.1749.v1

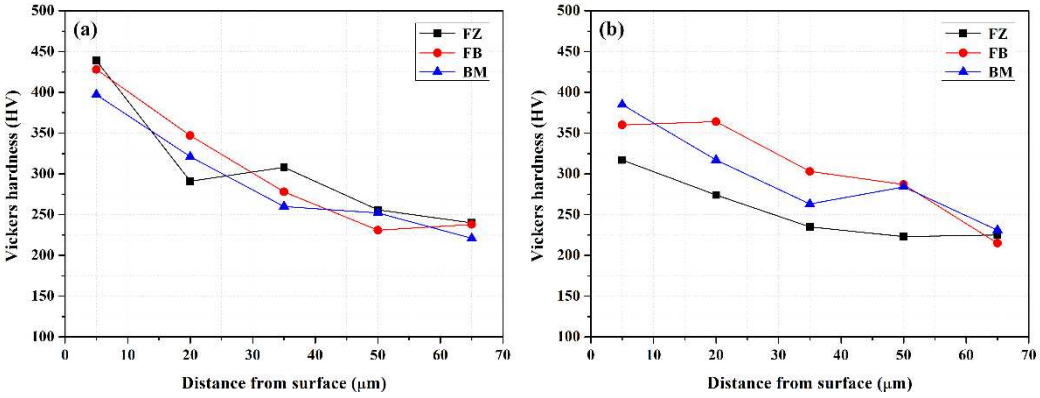

Figure 4. The changes in micro-hardness in the thickness direction in the BM, FB and FZ of the (**a**) 304RWSP and (**b**) 316RWSP samples from the shot-peened surface to the interior of the welds.

3.4. Surface appearance of the tested samples after salt spray

The surface appearances of distinct samples after salt spray are illustrated in Figure 5. As compared with the annealed plate [22], severe rusting in different patches with deep pits was seen in the 304R after salt spray (Figure 5a). However, rusting in the 316R after the test was moderate (Figure 5b), as compared with the 304R. Thus, cold rolling inevitably decreased the corrosion resistance of the ASS in a salt spray. The top appearance of the U-bend welds is shown in Figure 5c-d. The 304RW (Figure 5c) was rusting heavier than the 316RW (Figure 5d). It seemed that the FBs of the weld were corroded severer than the other zones of the weld. Obviously, the discontinuous profile at the FB might assist the accumulation of harmful species therein, resulting in heavy rusting. Moreover, the imposed welding heat on the cold-rolled SS plate will enhance the occurrence of sensitization in the heat-affected zone of an ASS weld [15-16]. Overall, the macro-appearance of the U-bend samples after salt spray was similar in each group with or without shot-peening. However, the corrosion pits and fine ditches were less likely to form in the 316RWSP sample.

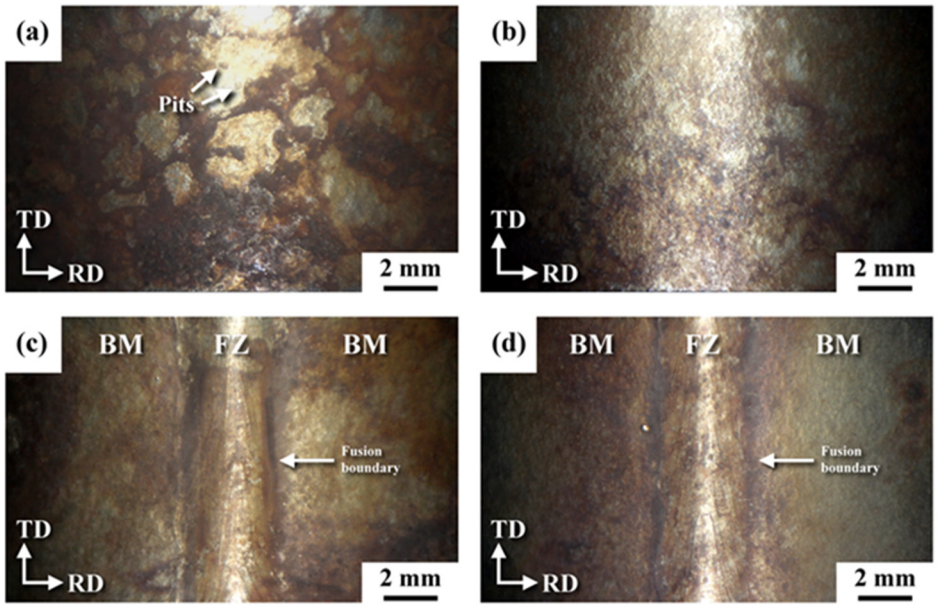

Figure 5. The macro-surface appearance of the U-bend samples for the (**a**) 304R, (**b**) 316R, (**c**) 304RW and (**d**) 316RW samples after salt spray.

SEM micrographs to display the surface morphology of the U-bend test pieces after salt spray is shown in Figure 6. The 304R corroded severely, which showed granular-like cracks inter-dispersed

Preprints (www.preprints.org) | NOT PEER-REVIEWED | Posted: 27 October 2023 doi:10.20944/preprints202310.1749.v1

with coarse pits (Figure 6a). In contrast, no granular-like cracks and small corrosion pits were seen in the 316R after salt spray (Figure 6b). After MSP, the corroded surface of the 304RSP sample showed the un-even size dents inter-dispersed with numerous microcracks (Figure 6c). By contrast, less rusty dents with sparse microcracks were observed in the 316RSP (Figure 6d). It was obvious that MSP was able to prevent the formation of coarse corrosion pits in the cold-rolled ASS.

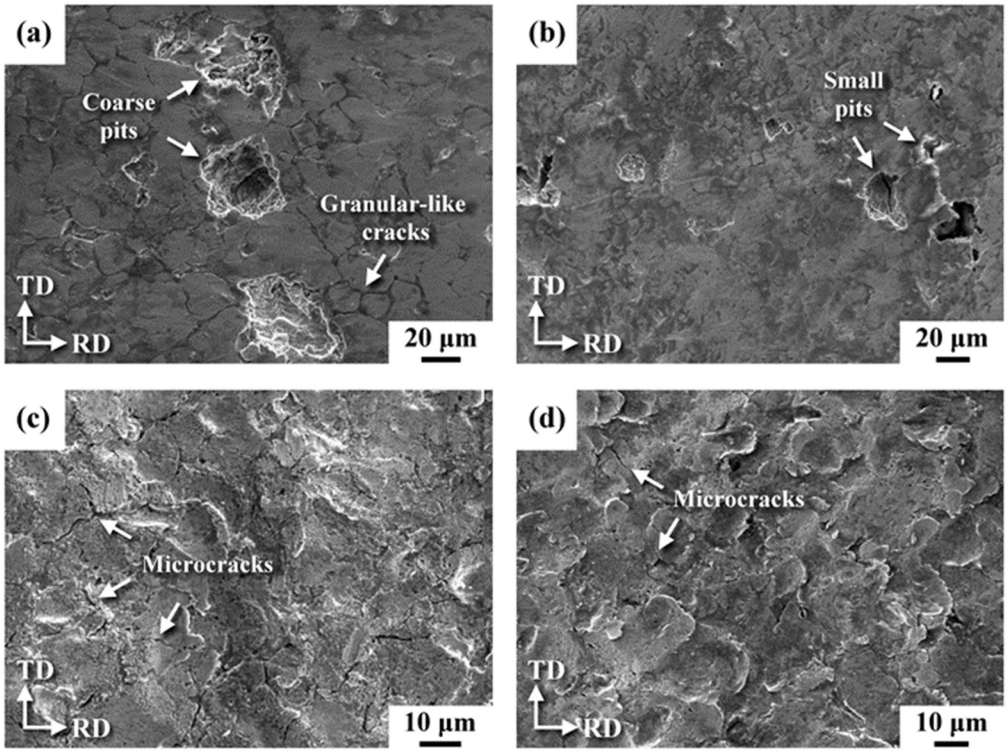

Figure 6. SEM micrographs showing the surface appearance of the (**a**) 304R, (**b**) 316R, (**c**) shot-peened 304R (304RSP) and (**d**) shot-peened 316R (316RSP) samples after salt spray.

Figure 7 shows the SEM morphology of the U-bend welds with or without MSP. Without MSP, the FB of the 304RW consisted of aligned corrosion pits and the FZ was also damaged by un-even sizes of corrosion pits (Figure 7a). Corrosion pits were less likely to be seen in the 316RW (Figure 7b) relative to those in the 304RW. Overall, corrosion damage seemed to be heavier at the FB than at other zones in the 316RW. With MSP, numerous fine dents and pits were formed around the FB of the 304RWSP after salt spray (Figure 7c). The corrosion pits of the peened 304RW (304RWSP) were finer but greater in amount than the un-peened one. Relatively coarse pits were found occasionally in the FZ of the 304RWSP sample. The feature of impact dents formed on the surface of the peened 316RW (316RWSP) was still visible in distinct zones (Figure 7d), which implied the less corroded surface after salt spray. With the discontinuous profile, the FB of the 316RWSP sample remained the weak sites for SCC relative to other zones. Overall, the better reliability and longer service life of dry storage canister could be achieved by using 316L SS for construction and application of MSP on it.

Preprints (www.preprints.org) | NOT PEER-REVIEWED | Posted: 27 October 2023 doi:10.20944/preprints202310.1749.v1

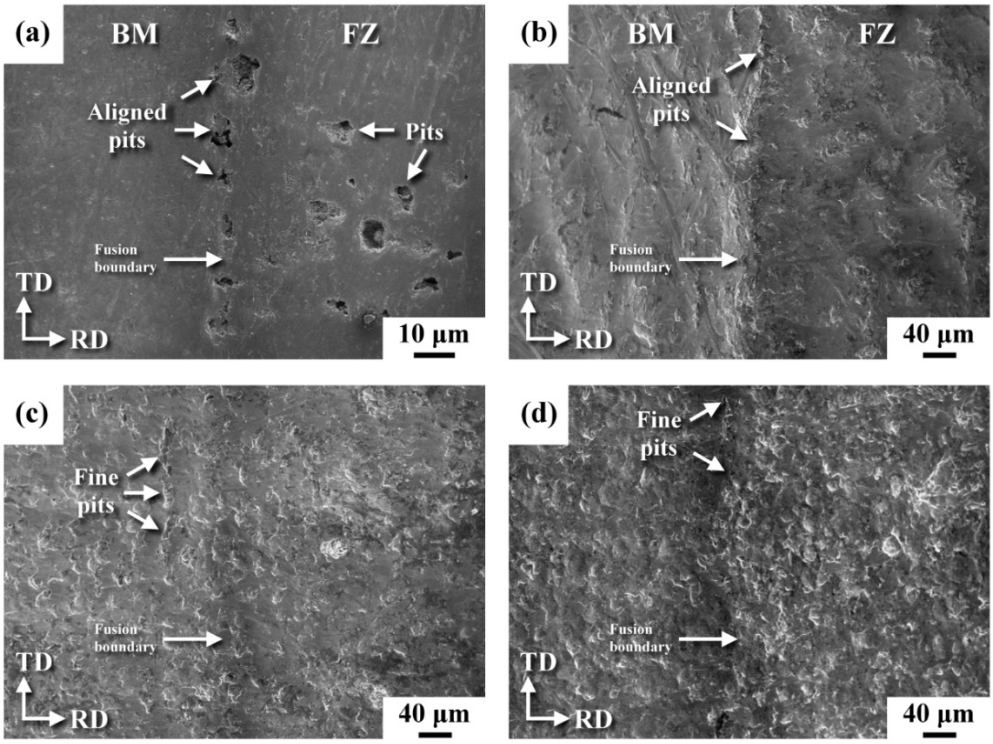

Figure 7. SEM morphologies of the (**a**) 304RW, (**b**) 316RW, (**c**) shot-peened 304RW (304RWSP) and (**d**) shot-peened 316RW (316RWSP) samples after salt spray.

3.5. XRD analysis of residual stress in the cold-rolled plates

Residual stress profiles along the thickness direction from the top to the interior of the 304R and 316R with or without MSP are shown in Figure 8. In prior work [22], residual stress profiles of the as-welded FZ along the thickness direction were determined after grinding off the weld reinforcement. The tensile stress state of the as-welded FZ changes into compressive state of about 750 MPa after MSP [22]. It was expected that residual tensile stress would increase the SCC susceptibility of the investigated sample, whereas residual compressive stress would mitigate the occurrence of SCC. As shown in Figure 8, the residual stress on the surface of the 304R and 316R was in tension and the peak tensile stress of those two samples was about 200 MPa. Residual tensile stress on the 304R and 316R was expected to increase their SCC susceptibility. However, residual compressive stress over -800 MPa was obtained for the peened 316R (316R+MSP) and -1100 MPa for the peened 304R (304R+MSP). Such high induced residual compressive stress after MSP could be related to shot-peening the cold-rolled plate and induced martensitic transformation in the peened zone. As shown in Figure 8, the narrow compressive stress field could be associated with the intense but limited depth of plastic deformation caused by MSP. In this work, the discontinuous profile made the stress measurements around the FZ impractical. However, introducing residual compressive stress by peening the weld was anticipated to lower the SCC susceptibility in different zones of an ASS weld.

Preprints (www.preprints.org) | NOT PEER-REVIEWED | Posted: 27 October 2023 doi:10.20944/preprints202310.1749.v1

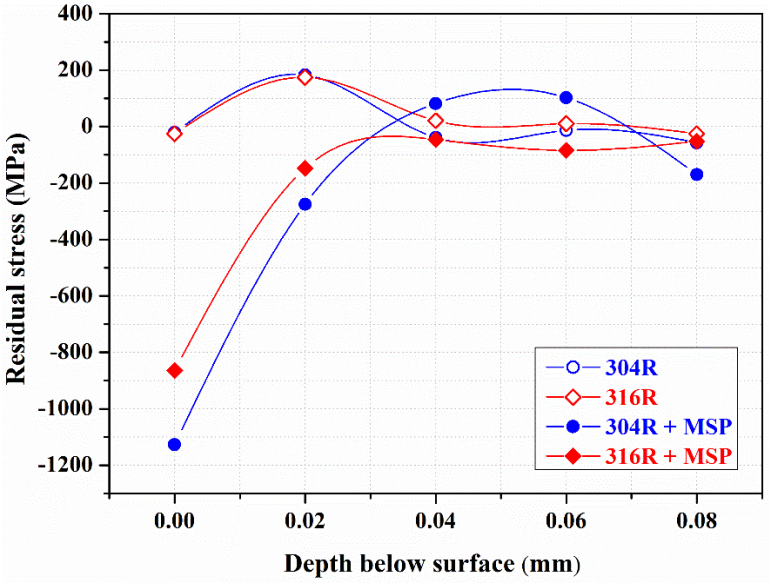

Figure 8. The residual stress profiles of the cold-rolled plates in the as-rolled and shot-peened conditions determined by XRD.

3.6. EBSD analysis of the U-bend welds

Figure 9 is the EBSD analysis showing the outermost microstructures in a cross sectional view in the BM zone of the peened U-bend weld. The results indicated that extensive slips (Figure 9a) and a great amount of induced α'-martensite (Figure 9c) were formed in the BM zone of the 304RW relative to those of the 316RW (Figure 9b, d). As compared with the counterpart sample in the annealed state [22], prior cold-rolling indeed assisted the occurrence of strain-induced transformation in the current weld. Those patches with dense slip bands were also accompanied with the presence of α'-martensite (Figure 9c) and high local strain (Figure 9e). By contrast, scarce slips (Figure 9b) and trivial martensite (Figure 9d) formed in the BM zone of the 316RWSP assured that the 316L was much stable and resistant to plastic deformation. Although all the external surface of the U-bend weld had been shot-peened, only a very thin surface layer showed refined structure and sparse martensite in the BM zone of the weld. It was deduced that the strain-hardening caused by prior cold-rolling of the substrate impeded the further plastic deformation of the ASS during MSP, resulting in showing limited peening effect.

After MSP, the EBSD investigations around the FB of the peened U-bend 304RW (304RWSP) in cross sectional view are shown in Figure 10. As revealed in Figure 10a-b, the zone near the FB on the BM side comprised similar microstructures as the BM, shown in Figure 9a, c. Owing to the coarse granular structure of the 304L substrate, the slip bands or lath martensite on the BM side were coarser and longer than those in the FZ (Figure 10a-b). It could be deduced that the fine δ-ferrite, solidified skeletal structure and induced fine martensite in the FZ were responsible for a finer lath microstructure than the zone on the BM side. It was noticed that the outer surface of the FZ was covered by thin but dense martensite (Figure 10b), whereas it was hard to observe on the BM side. Therefore, the FZ was more likely to undergo strain-induced transformation under shot-peening than the cold-rolled substrate. Moreover, the strain map (Figure 10c) also revealed that the FZ had high local strain relative to the zone on the BM side. Grain boundary (GB) map (Figure 10d) showed the grain boundary characteristics of the inspected sample. Low-angle grain boundaries (LAGBs) include the martensite lath and high density dislocation-tangled boundaries within the matrix. High-angle grain boundaries (HAGBs) are associated with γ, δ-ferrite and α'-martensite boundaries, having misorientations of 15-62.5° relative to the adjacent grains. In Figure 10d, the LAGBs are colored by red (1°-5°) and green (5°-15°) lines; HAGBs (15°-62.5°) are colored by black. The FZ consisted of higher density of LAGBs than the zone on the BM side, which implied the slips or dislocation motions were more likely to occur in the FZ during straining. Those fine dark spots could be related with the

Preprints (www.preprints.org) | NOT PEER-REVIEWED | Posted: 27 October 2023 doi:10.20944/preprints202310.1749.v1

induced α'-martensite or δ-ferrite. It was noted that the peened surface on the BM side comprised a very thin layer of refined structure with dense LAGBs (Figure 10d).

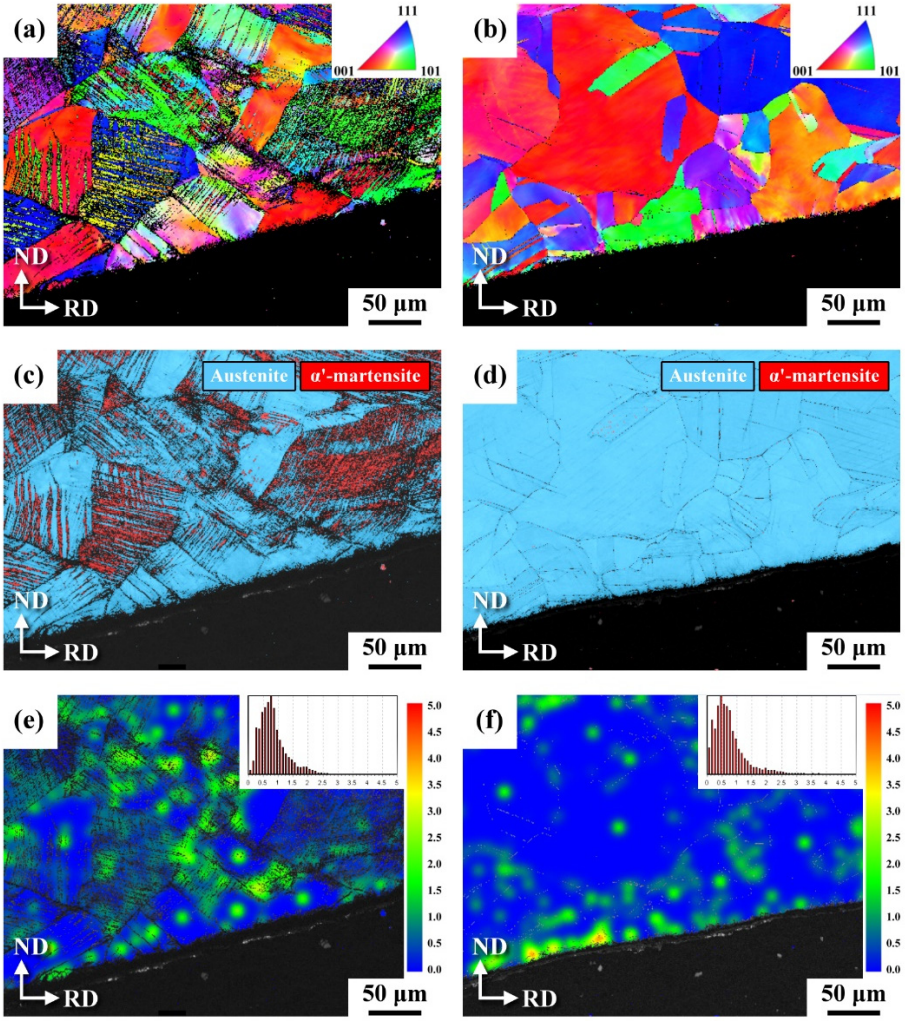

Figure 9. EBSD (**a**), (**b**) IPF maps, (**c**), (**d**) phase maps, (**e**), (**f**) strain maps in cross sectional view of the U-bend samples in the BM of (**a**), (**c**), (**e**) the 304RWSP; (**b**), (**d**), (**f**) the 316RWSP samples.

The EBSD investigations around the FB of the U-bend peened 316RW (316RWSP) in cross sectional view are shown in Figure 11. The FZ also had a finer structure than the zone on the other side of the FB (Figure 11a). According to the phase map (Figure 11b), the ferromagnetic phase present in the FZ of the 316RWSP was fewer and finer than that in the 304RWSP. As mentioned in the text, thin but dense α'-martensite was obtained in the heavily peened layer in the FZ of the 304RWSP. However, only rare martensite was detected on the top surface of the FZ in the 316RWSP under the same peening (Figure 11b). The result indicated that strain-induced transformation less occurred even in the solidified 316L. The strain map (Figure 11c) also displayed that the FZ of the 316RW was of high strain relative to that of the other zones, which should be inferior to the SCC resistance. The GB map of the 316RW (Figure 11d) showed the FZ consisted of refined structure or high GB densities relative to the zone on the BM side. Moreover, a quite difference in LAGBs in the FZ of the 304RW (Figure 10d) and 316RW (Figure 11d) was seen, which could be associated with fewer dislocation motions/slips in the latter during bending.

Preprints (www.preprints.org) | NOT PEER-REVIEWED | Posted: 27 October 2023 doi:10.20944/preprints202310.1749.v1

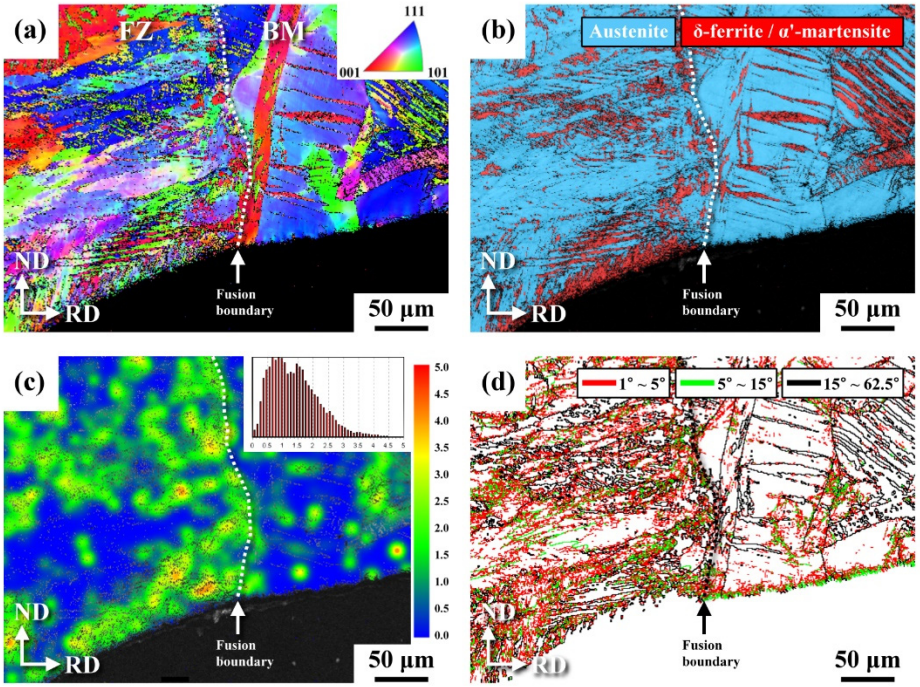

Figure 10. EBSD (**a**) IPF map, (**b**) phase map, (**c**) strain map, (**d**) GB map of the U-bend sample around the FZ of the 304RWSP sample in cross sectional view.

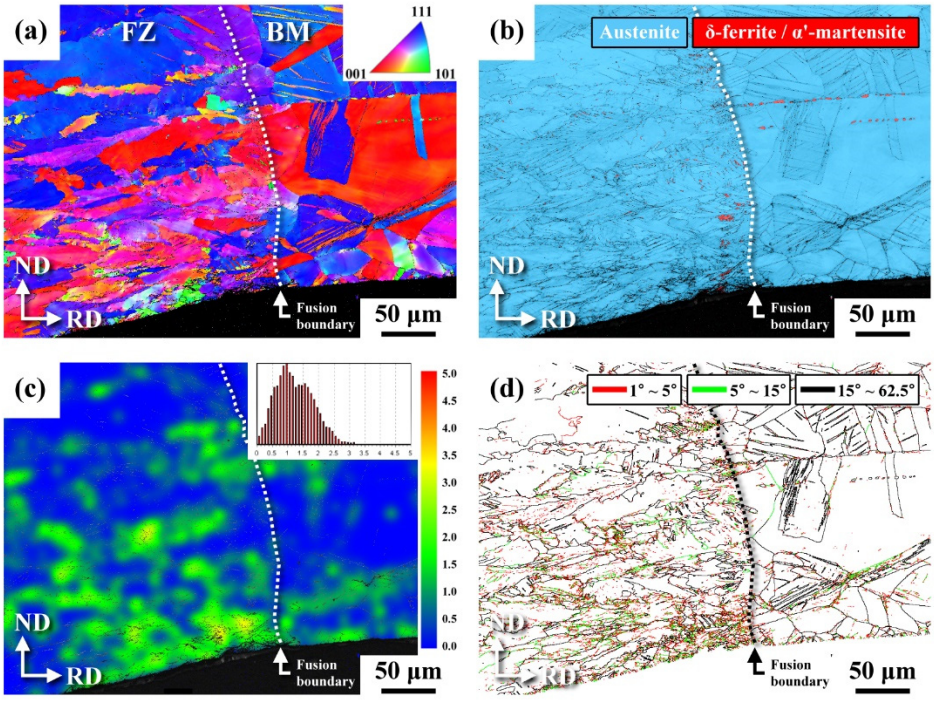

Figure 11. EBSD (**a**) IPF map, (**b**) phase map, (**c**) strain map, (**d**) GB map of the U-bend sample around the FZ of the 316RWSP sample in cross sectional view.

4. Discussion

The resistance to PTC and SCC is the great concerns of the dry canister for the storage of spent nuclear fuels near to the coast line. The combination of deformation-induced martensite and a large amount of MnS inclusion is reported to deteriorate the corrosion resistance of a 304 SS rod in a

 doi:10.20944/preprints202310.1749.v1

chloride environment [26]. Thus, machining process, welding, and microstructural heterogeneity present in the original SS plate may lower the reliability of the canister during long term service. In 1 M NaCl + 0.5 M HCl, the weld metal (WM) and heat affected zone (HAZ) of a 304 GTAW weld are more sensitive to PTC than the BM [28]. The HAZ of a 304 SS weld is pointed out to have high sensitivity to SCC in chloride solution [29,30]. Among the distinct zones in a 316 SS weld exposed to the synthetic sea-salt and $MgCl_2$ deposits, the HAZ showed high SCC relative to the WM and BM due to the combination of tensile residual stress and plastic strain [1]. Therefore, special concerns should be paid to mitigate PTC/SCC in the HAZ of a weld.

In this work, annealed 304L and 316L SS plates were cold-rolled to about 10 % reduction in thickness. The XRD spectrums (Figure 2) showed the results of little austenite transformation to martensite even for the cold-rolled 304L but caused slight strain-hardening. Residual stress profiles along the thickness direction from the top to the interior of the 304R and 316R samples were determined (Figure 8). The surface residual stress of the 304R and 316R was in tension and the peak tensile stress of those two samples was about 200 MPa. Therefore, cold-rolling introduced residual tensile stress into the SS plates, which was expected to increase the SCC susceptibility. By contrast, MSP reversed the residual stress profiles of the cold-rolled plates. Residual compressive stress over -800 MPa was introduced for the peened 316R (316RSP) and -1100 MPa for the peened 304R (304RSP). The corrosion resistance of the HAZ of the tungsten inert gas (TIG) welded 304 SS weld in NaCl solution is improved by increasing the welding current and number of passes; the causes are related to the decreased or relaxed residual stresses [27]. Therefore, it was practical to apply MSP after welding to reverse the surface tensile stress into compressive stress to lower the SCC susceptibility of an ASS weld in a chloride-containing environment.

Severe rusting of the 304R, which showed granular-like cracks inter-dispersed with coarse pits (Figure 6a), occurred after salt spray, whereas no granular-like cracks and fine corrosion pits were seen in the 316R. The FB of the 304RW consisted of aligned corrosion pits and the FZ was also damaged by un-even sizes of corrosion pits (Figure 7a). Moreover, the 304RSP displayed un-even size dents inter-dispersed with numerous microcracks (Figure 6c). By contrast, less corroded dents with sparse microcracks were observed in the 316RSP (Figure 6d). With MSP, numerous fine dents and pits were formed around the FB of the 304RWSP after salt spray (Figure 7c). The corrosion pits of the peened 304RW were finer but greater in amount than the un-peened one. It was obvious that the formation of coarse pits and linkage of coarse pits into a microcrack at the FB of an ASS weld could be mitigated by MSP. Therefore, applying MSP on a 316L SS canister would be better for storing spent nuclear fuels, which showed the increased reliability for long-term service in a chloride-containing environment.

The EBSD analysis revealed that those patches with dense slip bands also accompanied with the presence of α'-martensite (Figure 9c) and high local strain (Figure 9e). The FZ was shown to be of high shrinkage strain (Figure 9e). It was known that α'-martensite and high local strain was harmful to PTC and SCC resistance of an ASS. The top FZ surface of the 304RWSP was covered with dense but thin α'-martensite, which might impaire the PTC and SCC resistance. However, MSP resulted in forming refined microstructure and introducing huge residual compressive stress in the peened zone of an ASS, which were beneficial to impede the initiation of PTC and SCC. Overall, the harmful effect of α'-martensite on SCC resistance of an ASS was overcame by the positive effect of refined structure and residual compressive stress after MSP. Therefore, the SCC of the ASS welds could be effectively retarded by MSP, particularly for the 316L SS weld. High local strain at the FB was the reasons for the high SCC cracking in an ASS weld. Ultrasonic peening is applied to modify the weld toe geometry and introduces residual compressive stress into a 304 weld [21], which makes the corrosion resistance even better than the base metal. MSP could not correct the geometry of the weld toe. Without grinding off the weld reinforcement, MSP was still able to lower the SCC susceptibility of two ASS welds, in which the substrate was originally in the cold-rolled condition. Therefore, the application of MSP to reduce the SCC susceptibility of the canister for the storage of spent nuclear fuels was practical. In addition, the 316 canister with MSP would show the better service reliability to impede the incidence of PTC and SCC in a chloride-containing environment.

5. Conclusions

1. With a 10 % reduction in thickness after cold-rolling, even the 304R showed a minor amount of phase change and slight strain-hardening. However, cold-rolling introduced residual tensile stress into the SS plates, which would increase the PTC and SCC susceptibility. MSP assisted the austenite to martensite transformation, particularly the FZ of the 304RW. Moreover, MSP reversed the residual stress profiles of the cold-rolled plates. Residual compressive stress over -800 MPa was introduced for the peened 316R (316RSP) and -1100 MPa for the peened 304R (304RSP).
2. Severe rusting in the 304R was seen after salt spray, which showed granular-like cracks inter-dispersed with coarse corrosion pits. After MSP, the corroded surface of the peened 304R showed the un-even size dents inter-dispersed with numerous microcracks.
3. Without MSP, the FB of the 304RW consisted of aligned corrosion pits, whereas the FZ was also damaged by un-even sizes of corrosion pits. With MSP, numerous fine dents and pits were found around the FB of the 304RWSP after salt spray. The feature of impact dents formed on the peened 316RW (316RWSP) surface was visible in distinct zones, which implied the less damage after salt spray.
4. The high local strain and the existence of α'-martensite in the FZ deteriorated its PTC and SCC resistance. The peened FZ surface of the 304RWSP sample was covered with dense but thin α'-martensite, which increased the SCC susceptibility. However, the refined microstructure and high compressive residual stress introduced by MSP were beneficial to impede the initiation of PTC and SCC. The results indicated that the PTC and SCC susceptibility of an ASS weld could be lowered by MSP. The better reliability and longer service life of dry storage canister could be achieved by using 316L SS for construction and application of MSP on it.

Author Contributions: Chia-Ying Kang: Investigation, Data Curation; **Tai-Cheng Chen**: Investigation, Data curation, Writing - Review & Editing; **Ren-Kae Shiue:** Supervision, Writing - Review & Editing, Visualization; **Leu-Wen Tsay:** Conceptualization, Methodology, Resources, Writing - Original Draft, Project administration.

Funding: This research was funded by the Ministry of Science and Technology, R.O.C. (Contract No. MOST 109-2221-E-019-023-MY3)

Data Availability Statement: Data available on request due to restrictions e.g., privacy or ethical.

Acknowledgments: The authors would like to thank Likuan Technology Corp. for the great help of determining the residual stress of the investigated sample and Vincent Vacuum Tech. for performing the MSP.

Conflicts of Interest: The authors declare no conflict of interest.

References

1. Dong, P.; Scatigno, G.G.; Wenman, M.R. Effect of Salt Composition and Microstructure on Stress Corrosion Cracking of 316L Austenitic Stainless Steel for Dry Storage Canisters. J. Nucl. Mater. **2021**, 545, 152572.
2. Vehovar, L.; Tandler, M. Stainless steel containers for the storage of low and medium level radioactive waste. Nucl. Eng. Des. **2001**, 206, 21-23.
3. Kain, V.; Sengupta, P.; De, P.K.; Banerjee, S. Case reviews on the effect of microstructure on the corrosion behavior of austenitic alloys for processing and storage of nuclear waste. Metall Mater Trans A. **2005**, 36, 1075-1084.
4. Kim, S.; Kim, G.; Oh, C.Y.; Song, S. Pitting and Localized Galvanic Corrosion Characteristics of Gas Tungsten Arc Welded Austenitic Stainless Steel. Met. Mater. Int. **2022**, 28, 2448-2461.
5. Acharyya, S.G.; Khandelwal, A.; Kain, V.; Kumar, A.; Samajdar, I. Surface working of 304L stainless steel: Impact on microstructure, electrochemical behavior and SCG resistance. Mater Charact. **2012**, 72, 68-76.
6. Zhang, W.; Wang, X.; Hu, Y.; Wang, S. Quantitative Studies of Machining-Induced Microstructure Alteration and Plastic Deformation in AISI 316 Stainless Steel Using EBSD. J. Mater. Eng. Perform. **2018**, 27, 434-446.
7. Tsay, L.W.; Lin, Y.J.; Chen, C. The effects of rolling temperature and sensitization treatment on the sulfide stress corrosion cracking of 304L stainless steel. Corros Sci. **2012**, 63, 267-274.
8. Odnobokova, M.; Belyakov, A.; Enikeev, N.; Kaibyshev, R.; Valiev, R.Z. Microstructural Changes and Strengthening of Austenitic Stainless Steels during Rolling at 473 K. Metals. **2020**, 12, 1614.

9. Katsuyama, J.; Tobita, T.; Itoh, H.; Onizawa, K. Effect of Welding Conditions on Residual Stress and Stress Corrosion Cracking Behavior at Butt-Welding Joints of Stainless Steel Pipes. J Press Vessel Technol. **2012**, 134, 021403.
10. Wu, X. On residual stress analysis and microstructural evolution for stainless steel type 304 spent nuclear fuel canisters weld joint: Numerical and experimental studies. J. Nucl. Mater. **2020**, 534, 152131.
11. He, S.; Jiang, D. Effect of the Degree of Rolling Reduction on the Stress Corrosion Cracking Behavior of SUS 304 Stainless Steel. Int. J. Electrochem. Sci. **2018**, 13, 1614-1628.
12. Solomon, N.; Solomon, I. Effect of deformation-induced phase transformation on AISI 316 stainless steel corrosion resistance. Eng Fail Anal. **2017**, 79, 865-875.
13. Park, I.; Kim, E.Y.; Yang, W.J. Microstructural Investigation of Stress Corrosion Cracking in Cold-Formed AISI 304 Reactor. Metals. **2021**, 11, 7.
14. Ghosh, S.; Kain, V. Effect of surface machining and cold working on the ambient temperature chloride stress corrosion cracking susceptibility of AISI 304L stainless steel. Mater. Sci. Eng. A. **2010**, 527, 679-683.
15. Kain, V.; Chandra, K.; Adhe, K.N.; De, P.K. Effect of cold work on low-temperature sensitization behaviour of austenitic stainless steels. J. Nucl. Mater. **2004**, 334, 115-132.
16. Singh, R. Influence of cold rolling on sensitization and intergranular stress corrosion cracking of AISI 304 aged at 500 °C. J Mater Process Technol. **2008**, 206, 286-293.
17. Li, W.J.; Young, M.C.; Lai, C.L.; Kai, W.; Tsay, L.W. The effects of rolling and sensitization treatments on the stress corrosion cracking of 304L stainless steel in salt-spray environment. Corros Sci. **2013**, 68, 25-33.
18. Lu, Z.; Xu, F.; Tang, C.; Cui, Y.; Xu, H.; Mao, J. Stress Corrosion Cracking Susceptibility of 304 Stainless Steel Subjected to Laser Shock Peening without Coating. J. Mater. Eng. Perform. **2021**, 30, 7163-7170.
19. Liu, H.; Wei, Y.; Tan, C.K.I.; Ardi, D.T.; Tan, D.C.C.; Lee, C.J.J. XRD and EBSD studies of severe shot peening induced martensite transformation and grain refinements in austenitic stainless steel. Mater Charact. **2020**, 168, 110574.
20. Ye, C.; Telang, A.; Gill, A.; Wen, X.; Mannava, S.R.; Qian, D.; Vasudevan, V.K. Effects of Ultrasonic Nanocrystal Surface Modification on the Residual Stress, Microstructure, and Corrosion Resistance of 304 Stainless Steel Welds. Metall Mater Trans A. **2018**, 49, 972-978.
21. Abdullah, A.; Malaki, M.; Eskandari, A. Strength enhancement of the welded structures by ultrasonic peening. Mater. Des. **2012**, 38, 7-18.
22. Kang, C.Y.; Chen, T.C.; Tsay, L.W. Effects of Micro-Shot Peening on the Stress Corrosion Cracking of Austenitic Stainless Steel Welds. Metals. **2023**, 13, 69.
23. Hensel, J,; Eslami, H; Nitschke-Pagel, T.; Dilger, K. Fatigue strength enhancement of butt welds by means of shot peening and clean blasting. Metals. **2019**, 9, 744.
24. Muñoz, J.A.; Dolgach, E.; Tartalini, V.; Risso, P.; Avalos, M.; Bolmaro, R.; Cabrera, J.M. Microstructural Heterogeneity and Mechanical Properties of a Welded Joint of an Austenitic Stainless Steel. Metals. **2023**, 13, 245.
25. Chung, Y.-H.; Chen, T.-C.; Lee, H.-B.; Tsay, L.-W. Effect of Micro-Shot Peening on the Fatigue Performance of AISI 304 Stainless Steel. Metals **2021**, 11, 1408.
26. Sharma, P.; Roy, H. Pitting corrosion failure of an AISI stainless steel pointer rod. Eng. Fail. Anal. **2014**, 44, 400-407.
27. Lu, B.-T.; Chen, Z.-K.; Luo, J.-L.; Patchett, B. M.; Xu, Z.-H. Pitting and stress corrosion crack behavior in welded austenitic stainless steel. Electrochimical Acta. **2005**, 50, 1391-1403.
28. Franco, C. V.; Barbosa, R.P.; Martinelli, A.E.; Buschinelli, A.J.A. Study of the influence of welding parameters on the stress corrosion resistance of AISI 304 steel. Mats. Corro. **1998**, 49, 496-504.
29. Kessal, B. A.; Fares, C.; Meliani, M. H.; Alhussein, A.; Bouledroua, O.; Francois, M. Effect of gas tungsten arc welding parameters on the corrosion resistance and the residual stress of heat affected zone. Eng. Fail. Anal. **2019**, 107, 104200.
30. Lu, B.-T.; Chen, Z.-K.; Luo, J.-L.; Patchett, B. M.; Xu, Z.-H. Stress corrosion crack initiation and propagation in longitudinally welded 304 austenitic stainless steel. Corro. Eng. Sci. Tech. **2003**, 38, 69-75.